Pergamon

Geochimica et Cosmochimica Acta, Vol. 66, No. 18, pp. 3235–3245, 2002

0016-7037/02 $22.00 + .00

PII S0016-7037(02)00927-4

Equilibrium and kinetic aspects of soddyite dissolution and secondary phase precipitation in aqueous suspension

DANIEL E. GIAMMAR† and JANET G. HERING*

California Institute of Technology, 1200 E. California Blvd., Environmental Engineering Science (138-78), Pasadena, CA 91125, USA

(*Received March* 20, 2001; *accepted in revised form April* 22, 2002)

Abstract—The dissolution and transformation of soddyite ($[UO_2]_2SiO_4 \cdot 2H_2O$) have been examined in aqueous suspension at pH 6 and 0.01 M $NaNO_3$. Soddyite is an important component of the paragenetic sequence of secondary minerals that arises from the weathering of uraninite ore deposits and corrosion of spent nuclear fuel. A soddyite of high purity and crystallinity was synthesized in the laboratory for use in dissolution experiments. In batch experiments, rapid dissolution occurred over an initial period of several hours followed by continuing steady-state dissolution for up to 700 h. Up to 200 h, U and Si were released into solution at their stoichiometric 2:1 ratio in soddyite. A decrease in the dissolved U concentration was observed at longer times, indicating the precipitation of a new phase. Even after precipitation of the secondary phase, the continuing dissolution of soddyite could be inferred from increasing dissolved Si concentrations. Through the use of X-ray diffraction, Raman spectroscopy, and scanning electron microscopy, the precipitated phase was identified as a clarkeite-like sodium uranyl oxide hydrate. The sodium uranyl oxide hydrate was ultimately the solubility-controlling solid, despite being only a minor component. Soddyite dissolution rates were quantified in flow-through experiments, in which reaction products were flushed from the reactors, thereby avoiding reprecipitation of U. The measured dissolution rate at pH 6 was 0.71 μmol U m^{-2} h^{-1}. A slower dissolution rate of 0.44 μmol U m^{-2} h^{-1} was observed when 100 μM dissolved Si was added to the reactor influent.

1. INTRODUCTION

Uranium(VI) is an integral structural constituent of a wide variety of minerals, of which the vast majority exhibit sheet structures. In contrast, the uranyl orthosilicate mineral soddyite, $(UO_2)_2SiO_4 \cdot 2H_2O$, has a framework structure. In all U(VI) minerals, the nearly linear structure of the uranyl cation (UO_2^{2+}) is retained, and the (uranyl) oxygen atoms occupy the axial positions in bipyramidal uranyl polyhedra (Burns, 1999). Because of the uncommon framework structure of soddyite, in which chains of pentagonal uranyl bipyramids are cross-linked by silicate tetrahedra, it is unlikely that the occurrence of soddyite in a paragenetic sequence with other uranyl minerals results from the reordering of the structure of the reacting solid phases.

Uranyl oxide hydrate and uranyl silicate minerals are the most common secondary phases formed during the oxidative weathering of uraninite (UO_2) (Finch and Murakami, 1999) and the U(IV) oxides that are the dominant component of spent nuclear fuel (Wronkiewicz and Buck, 1999). Precipitation of soddyite may be kinetically favored over precipitation of other uranyl silicates, such as uranophane ($Ca[UO_2]_2[SiO_3OH]_2 \cdot 5H_2O$), even when soddyite is not the predicted equilibrium phase under the prevailing geochemical conditions (Pearcy et al., 1994). Soddyite can also be formed by the alteration of previously precipitated uranophane upon exposure to dilute meteoric waters. In natural environments, soddyite is stable when in contact with waters high in dissolved silica, low in carbonate, and with a pH below 7 (Finch and Murakami, 1999).

Dissolution of U(IV) oxides and spent nuclear fuel controls the initial release of U and associated radionuclides from the solid phase (Shoesmith, 2000). Subsequently, the dissolved concentrations and hence the mobility of U and associated radionuclides may be limited by the solubility of secondary uranyl phases (Finn et al., 1996; Trocellier et al., 1998). A simple thermodynamic model of the dissolution of U(IV) oxide in granitic groundwater suggested that under oxidizing conditions, the solubility of U may be controlled by several uranyl phases, including soddyite (Trocellier et al., 1998). In unsaturated corrosion tests of both uraninite and spent nuclear fuel with groundwater from the Nevada Test Site adjacent to the proposed Yucca Mountain geologic repository for nuclear waste, soddyite was identified in the paragenetic sequence of alteration phases, which progressed from uranyl oxide hydrates to alkali uranyl silicates over a 10-yr experiment (Wronkiewicz and Buck, 1999; Wronkiewicz et al., 1992, 1996). Soddyite was observed as an abundant phase from 2 to 3.5 yr, succeeding the calcium uranyl oxide hydrate becquerelite and preceding the formation of the alkali uranyl silicates uranophane and boltwoodite. At the most comparable natural analog to the Yucca Mountain site, the Nopal I uranium deposit in Mexico, soddyite was observed in a similar progression of phases. While secondary mineralization is dominated by uranophane at the Nopal I site, the second most abundant uranyl silicate phase is soddyite. A progression from uranyl oxide hydrates (primarily schoepite) to uranyl silicates is clearly observed. Soddyite, however, does not appear to be a requisite intermediate phase between schoepite and uranophane; rather, the local geochemical conditions determine which specific uranyl silicates are formed (Ildefonse et al., 1990; Pearcy et al., 1994). Seepage

* Author to whom correspondence should be addressed (jhering@caltech.edu).

†*Present address:* Princeton University, Department of Geosciences, B73 Guyot Hall, Princeton, NJ 08544, USA.

waters from uranium mines in Germany contain elevated dissolved concentrations of both U and Si, and the solubility of uranyl silicates may be important in controlling U mobilization from these mines (Moll et al., 1996).

While the dissolution of uraninite has been studied under a variety of conditions (Casas et al., 1998; de Pablo et al., 1999; Steward and Mones, 1997; Torrero et al., 1994), information on the solubilities and dissolution rates of secondary uranyl minerals is limited. Some laboratory studies of synthetic soddyite phases have been performed in recent years. Methods of synthesis and characterization of soddyite have been discussed by Moll et al. (1995) and Vochten et al. (1995). The solubility of soddyite has been measured in dilute aqueous solution (Nguyen et al., 1992); 0.1 M $NaClO_4$ (Moll et al., 1996); and in the presence of dissolved Si, Na, and HCO_3^- (Pérez et al., 1997).

The solubility of soddyite has been determined in several studies, but the time scales of soddyite dissolution and the potential formation of secondary phases have not been extensively studied. The evolution of dissolved U concentrations over time was measured in two batch studies of soddyite dissolution (Moll et al., 1996; Pérez et al., 1997). On the basis of the observation of a transient peak in dissolved U concentrations, Moll et al. (1996) suggested that some alteration phases might have formed in systems open to the atmosphere. However, soddyite was identified as the solubility-controlling solid phase by X-ray diffraction (XRD). In the batch dissolution studies of Pérez et al. (1997), the formation of secondary solid phases was prevented by the presence of HCO_3^-.

In the current study, the dissolution and transformation of soddyite were investigated in complementary batch and flow-through experiments conducted at near-neutral pH. In batch experiments, the influence of the formation of secondary phases on the time evolution of dissolved U concentrations was elucidated by combining macroscopic observations of bulk solution chemistry with characterization of the reacting solid phase(s). Interpretation of observed rates of U and Si release, however, was complicated by the accumulation of reaction products and the formation of secondary phases. The coexistence of soddyite and a sodium uranyl oxide hydrate secondary phase was demonstrated by XRD, Raman spectroscopy, and scanning electron microscopy (SEM). The range of the solubility product of the secondary phase that would allow its coexistence with soddyite under the conditions of the batch experiments was determined through equilibrium calculations. Soddyite dissolution rates were quantified in flow-through experiments in which secondary phase formation was avoided by the continuous removal of reaction products.

2. EXPERIMENTAL MATERIALS AND METHODS

2.1. Soddyite Synthesis

Soddyite was synthesized by the method of Moll et al. (1995), which had been optimized for yield and phase purity. Two separate batches (syntheses 1 and 2) were prepared by combining stoichiometric amounts of 0.1 M $UO_2(CH_3COO)_2 \cdot 2H_2O$ (Alfa Aesar) and 0.1 M $Na_2SiO_3 \cdot 5H_2O$ (Alfa Aesar) solutions in the Teflon liner of a 23-mL Parr bomb. The Parr bomb was heated to 110°C for 10 d and then cooled. The precipitated solids were filtered with a 0.2-μm polycarbonate filter membrane (Millipore Corp.) and then washed with boiling deionized water to remove any excess reactants. The remaining solids were rinsed off of each filter and diluted to stock suspension volumes of ~20 mL with deionized water. The mass concentration of soddyite in each suspension was determined gravimetrically by filtering an aliquot of the suspension through preweighed polycarbonate filter membranes, drying, and weighing the filter and solids.

2.2. Dissolution Experiments

Soddyite dissolution was investigated in both batch and flow-through modes. All dissolution experiments were conducted at the ambient temperature of the laboratory (22 ± 2°C). Duplicate batch experiments were initiated by adding a volume of stock soddyite suspension to a polycarbonate flask containing a magnetically stirred solution of 5 mM 2-(n-morpholino)ethanesulfonic acid (MES) buffer (Avocado Research Chemicals) in 0.01 M $NaNO_3$ (Mallinckrodt). The pH of the solutions was adjusted to 6.00 with NaOH before the soddyite addition, contributing an additional 2.3 mM Na to the system. The solution pH was chosen because at pH 6, there is limited formation of uranyl-carbonate species (at most, 2.0% of dissolved U), because of the influence of atmospheric carbon dioxide. The MES buffer was chosen because of its demonstrated lack of metal complexation (Good et al., 1966; Soares et al., 1999). The pH was monitored during the addition of soddyite to the batch reactors to verify that the pH did not deviate from 6.00. Subsequent pH measurements were unnecessary because the strong buffering capacity of 5 mM MES at this pH was sufficient to maintain the pH within 0.01 pH units, given the small change in alkalinity associated with soddyite dissolution and uranyl hydrolysis for the maximum observed U release (10 μM). The flasks were allowed to equilibrate with atmospheric CO_2 both before and after soddyite addition but were capped during the course of the dissolution experiment to minimize evaporation. The batch reactors were periodically sampled to determine dissolved U and Si concentrations, to determine total U concentration, and to collect solids for subsequent analyses. Samples for dissolved U were collected by filtering 5 mL of suspension through 0.2-μm polycarbonate filter membranes (Millipore Corp.), collecting the last 1 mL of filtrate, and diluting 0.5 mL of the collected filtrate to 5 mL in 1% HNO_3. The filter membranes were removed from their filter holders, mounted on glass slides, air dried, and saved for XRD and SEM analyses. Samples for total U determination were obtained by diluting 0.5 mL of the unfiltered suspension to 10 mL with 10% HNO_3 to dissolve the soddyite particles.

In flow-through experiments, stock soddyite suspension was added to two ~50-mL polymethylmethacrylate stirred flow-through reactors with outlets sealed by 0.2-μm polycarbonate filter membranes to yield a soddyite concentration of 0.41 to 0.42 g L^{-1}. The exact volumes of the flow-through reactors were determined gravimetrically by filling them with water. The influent solutions for both flow-through reactors were 0.01 M $NaNO_3$ and 5 mM MES at pH 6.00, amended for one reactor to 100 μM Si (1 g L^{-1} Si standard, Aldrich). Flow to the reactors was controlled by a peristaltic pump, and stirring was provided by a magnetic stir bar and stir plate. The outflow of the reactors was monitored, and measured flow rates were used

to calculate residence times of 1.14 to 1.26 h for the reactor without added Si and 1.22 to 1.88 h (but mostly 1.22 to 1.44 h) for the reactor with added Si. The pH of the reactor effluents was also monitored.

Steady-state dissolution rates (μmol m^{-2} h^{-1}) were calculated as U release rates using the following equation:

$$\text{Rate} = \frac{C}{t_{res}} \frac{1}{S \cdot A} \quad (1)$$

where C is the effluent U concentration (μM), t_{res} is the hydraulic residence time of the reactor (h), S is the mass concentration of soddyite in the reactor (g L^{-1}), and A is the specific surface area (m^2 g^{-1}). After allowing the passage of 10 reactor volumes to establish hydrodynamic steady state, the dissolution rate was calculated for each effluent sample collected, and these values were averaged.

2.3. Analytical Methods

U and Si concentrations in solution were determined by inductively coupled plasma mass spectrometry (ICP-MS) with a Hewlett Packard HP4500 instrument. Thallium was used as an internal standard in ICP-MS analyses to compensate for drift in instrument sensitivity. Calibration was performed with commercially available standard solutions for U (Alfa Aesar), Si (Aldrich), and Tl (SPEX Chemical). Measurements of pH were made with a Ross glass electrode and Orion 720A pH meter.

The synthesized and partially-reacted solids were characterized and identified by powder XRD, diffuse reflectance infrared spectroscopy (DRIFTS), SEM, Raman spectroscopy, and Brunauer-Emmett-Teller (BET) surface area analysis. XRD analyses were performed on a Scintag Pad V X-ray powder diffractometer with a CuKα X-ray source and germanium detector. A Bio-Rad FTS-45 Fourier transform infrared spectrometer was used with a DRIFTS sample stage for infrared spectroscopy. Powdered soddyite was diluted with KBr before DRIFTS analysis. SEM images were collected on gold-coated samples with a Camscan Series II scanning electron microscope. Raman spectra were measured with a 514.5-nm argon ion laser on a Renishaw micro-Raman spectrometer with a spectral resolution of 1 cm^{-1}. Samples for Raman analysis were prepared by evaporating an aliquot of concentrated suspension on glass microscope slides. The surface area was determined on freeze-dried samples by BET N_2 adsorption using a Micromeritics Gemini surface area analyzer.

2.4. Equilibrium Calculations

Equilibrium calculations were performed with the program MINEQL$^+$ using the Davies (1962) equation to make ionic strength corrections (Environmental Research Software, 1998). The database of thermodynamic constants of dissolved uranyl species used in calculations (Table 1) is taken from the critical review of Grenthe et al. (1992), amended to use the $UO_2(OH)_2$(aq) formation constant of Silva (1992) and the $UO_2H_3SiO_4^+$ formation constant of Satoh and Choppin (1992). Calculations considered 10 hydrolysis reactions, 4 carbonate complexation reactions, and 1 silicate complexation reaction involving the uranyl cation. Species accounting for >2% of the dissolved U at pH 6, 0.012 M ionic strength, <10 μM $[U]_T$, 100 μM $[Si]_T$, and $10^{-3.5}$ atm CO_2 partial pressure are listed in boldface type in Table 1. While it is possible that not all of the reactors were in equilibrium with atmospheric CO_2 ($10^{-3.5}$ atm), the equilibrium speciation calculations made with this assumption yield an upper limit of 2.0% for the contribution of uranyl-carbonate species to the total dissolved U. For systems undersaturated with respect to atmospheric CO_2, the contribution of uranyl-carbonate species would be even less.

Table 1. Aqueous phase U(VI) reactions and thermodynamic stability constants considered in this work. Listed in bold face type are species that account for >2% of the total dissolved U at pH 6.0, 0.012 M ionic strength, 100 μM $[Si]_T$, $P_{CO2} = 10^{-3.5}$ atm, 25°C, and total U concentrations <10 μM. Log K values are reported for infinite dilution, and activity corrections for ionic strength effects were made using the Davies (1962) equation.

Reaction	Log K
$UO_2^{2+} + H_2O = UO_2OH^+ + H^+$	–5.20
$UO_2^{2+} + 2H_2O = UO_2(OH)_2(aq) + 2H^+$	–11.5[a]
$UO_2^{2+} + 3H_2O = UO_2(OH)_3^- + 3H^+$	–19.2
$UO_2^{2+} + 4H_2O = UO_2(OH)_4^{2-} + 4H^+$	–33.0
$2UO_2^{2+} + H_2O = (UO_2)_2OH^{3+} + H^+$	–2.7
$2UO_2^{2+} + 2H_2O = (UO_2)_2(OH)_2^{2+} + 2H^+$	–5.62
$3UO_2^{2+} + 4H_2O = (UO_2)_3(OH)_4^{2+} + 4H^+$	–11.9
$3UO_2^{2+} + 5H_2O = (UO_2)_3(OH)_5^+ + 5H^+$	–15.55
$3UO_2^{2+} + 7H_2O = (UO_2)_3(OH)_7^- + 7H^+$	–31.0
$4UO_2^{2+} + 7H_2O = (UO_2)_4(OH)_7^+ + 7H^+$	–21.9
$UO_2^{2+} + CO_3^{2-} = UO_2CO_3(aq)$	9.68
$UO_2^{2+} + 2CO_3^{2-} = UO_2(CO_3)_2^{2-}$	16.94
$UO_2^{2+} + 3CO_3^{2-} = UO_2(CO_3)_3^{4-}$	21.60
$3UO_2^{2+} + 6CO_3^{2-} = (UO_2)_3(CO_3)_6^{6-}$	54.0
$UO_2^{2+} + H_4SiO_4(aq) = UO_2H_3SiO_4^+ + H^+$	–2.5[b]

Sources: Grenthe et al. (1992); with the exceptions of [a]Silva et al. (1992) and [b]Satoh and Choppin (1992).

3. RESULTS

3.1. Soddyite Characterization

The powder XRD patterns of the synthesized solids are matched best by card 35-733 of the Joint Committee on Powder Diffraction Standards database (Fig. 1), which is labeled as soddyite (Joint Committee on Powder Diffraction Standards–International Centre for Diffraction Data, 1999). The DRIFTS spectrum obtained for the synthesized solids (Fig. 2) agrees very well with previously collected and interpreted spectra for synthetic soddyite (Moll et al., 1995; Cejka, 1999). Symmetric and antisymmetric stretching vibrations are observed at 834 and 912 cm^{-1}, respectively, for the uranyl ion and at 879 and 962 cm^{-1}, respectively, for the silicate ion. The sharp absorption peak at 1583 cm^{-1} is due to the bending vibration of water. The specific surface area of the synthesized soddyite was 3.15 m^2 g^{-1}.

3.2. Batch Dissolution Experiments

3.2.1. Solution chemistry

The evolution of the dissolved U and Si concentrations during batch soddyite dissolution is presented in Figure 3. Data were collected in two duplicate experiments, one with 0.13 g L^{-1} of soddyite from synthesis 1 and the other with 0.12 g L^{-1}

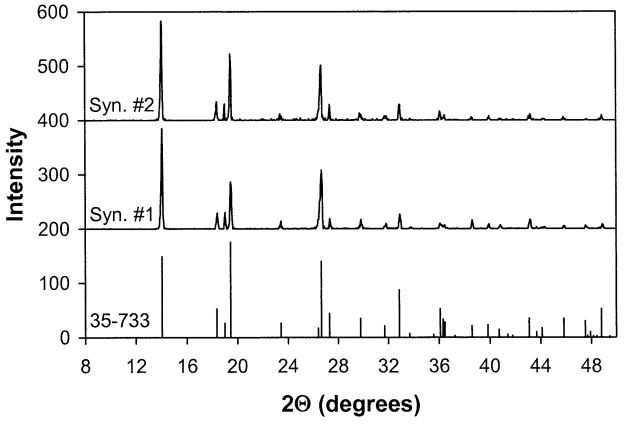

Fig. 1. X-ray diffraction patterns of synthetic soddyite and the Joint Committee on Powder Diffraction Standards–International Centre for Diffraction Data reference file (card 35-733) for soddyite.

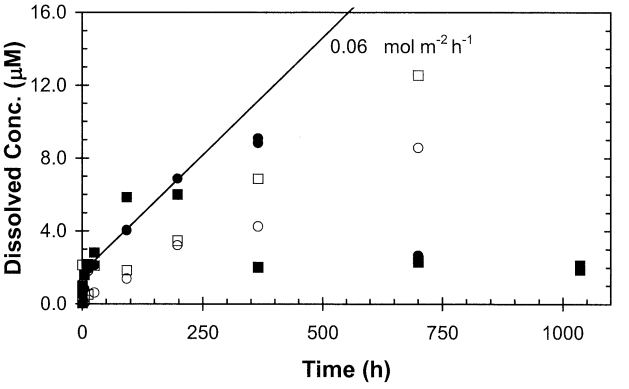

Fig. 3. Batch dissolution of soddyite (~0.125 g L^{-1}) at pH 6 (5 mM 2-[n-morpholino]ethanesulfonic acid) and I = 0.01 M ($NaNO_3$). Dissolved concentrations of U (●, ■) and Si (○, □) for both syntheses 1 (●, ○) and 2 (■, □). The line represents the expected U concentration for a dissolution rate of 0.064 μmol m^{-2} h^{-1} in the synthesis 1 reactor.

of soddyite from synthesis 2. The dissolved U concentration reached 1 μM after only 4 h and then increased at a slower rate from 4 h until 365 or 198 h for the soddyite from syntheses 1 and 2, respectively. A linear fit of the U data from 4 to 198 h (r^2 = 0.88) gives a U release rate of 0.064 μmol m^{-2} h^{-1} (shown by the line in Figure 3 for the 0.13 g L^{-1} flask).

The increase in the dissolved U concentration in the batch reaction flasks ceased sometime between 365 and 700 h for synthesis 1 and between 198 and 365 h for synthesis 2. The dissolved U concentration then decreased and remained constant in the range from 1.9 to 2.5 μM for the remainder of the experiment (1683 h). The decrease and stabilization of the dissolved U concentration suggest the precipitation of a new solubility-controlling phase.

In addition to the dissolved U concentration, the dissolved Si concentrations were also measured for the first 700 h of the experiment (samples collected after 700 h were lost during an unsuccessful ICP-MS run). The Si data can be fit linearly (r^2 = 0.89) for the data from 90 to 700 h to yield a Si release rate of 0.035 μmol m^{-2} h^{-1}. For samples obtained before the precipitation event, the ratio of dissolved U to Si is ~2 (Fig. 4), consistent with congruent dissolution.

The total U concentration of the suspension was monitored to check for the loss of U (solid or dissolved) to the container walls. The total U concentration remained near its expected value of 390 μM for synthesis 1 for the first 365 h and to the expected value of 360 μM for synthesis 2 for the first 198 h. After those times, the concentration began dropping, which indicates that some of the solid phase was adhering to the walls of the flasks. This phenomenon was also observed by visual examination of the reaction flasks.

3.2.2. Characterization of partly reacted solids

Solids were retained at each sampling point and analyzed. XRD patterns for the stock soddyite (synthesis 1) and for the solids in the reactor at several sampling times are shown in Fig. 5. XRD patterns were collected for solids retained on 0.2-μm

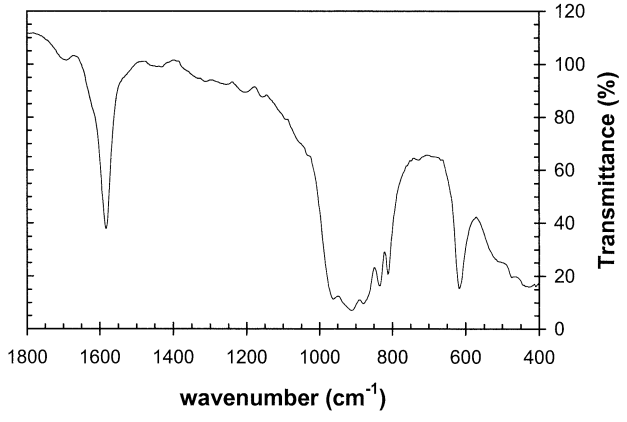

Fig. 2. Diffuse reflectance infrared spectroscopy spectrum of synthetic soddyite. Uranyl vibrations are observed at 834 cm^{-1} (symmetric) and 912 cm^{-1} (antisymmetric). Silicate vibrations are observed at 879, 960, and 619 cm^{-1}. The bending vibration of water gives rise to the strong peak at 1583 cm^{-1}.

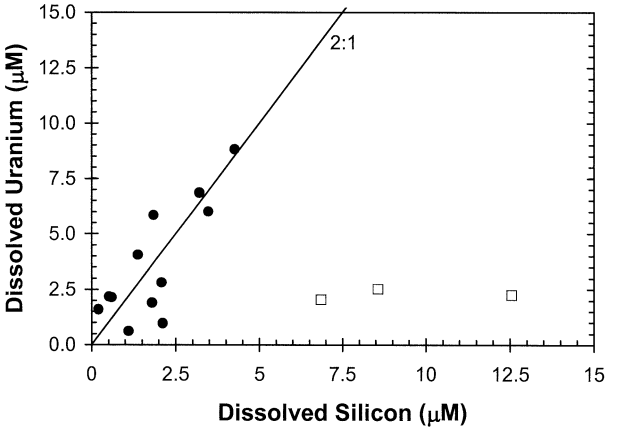

Fig. 4. Dissolved U vs. Si concentrations during batch soddyite dissolution. Data are shown for the period before (●) and after (□) the U reprecipitation event. The line corresponding to a 2:1 ratio of the U to Si concentrations represents ideal congruent dissolution.

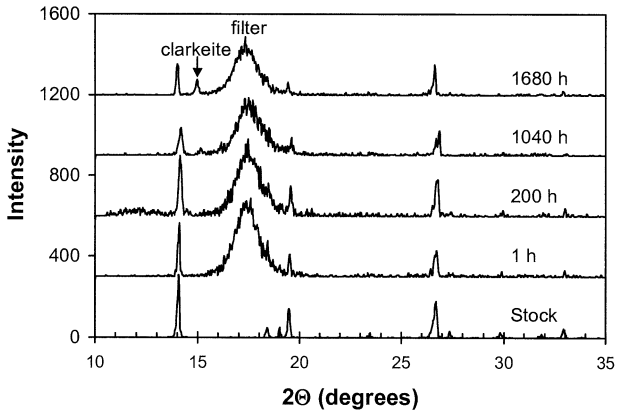

Fig. 5. Time series of X-ray diffraction patterns for solids collected from batch soddyite dissolution experiments. The three dominant peaks in the pattern for the stock soddyite (bottom pattern) are located at 14.1, 19.5, and 26.7°. The solids collected from 1 to 1680 h are impacted on polycarbonate filter membranes, which give rise to a broad peak from 16 to 19°. The peak appearing at 15.0° in the 1040- and 1680-h samples is a strong peak in the diffraction pattern of clarkeite.

polycarbonate filter membranes, which produce a broad peak observed at 16 to 19°. The dominant peaks of the stock soddyite are present in all of the samples of solids collected during batch dissolution. A peak at 15°, not seen for the stock soddyite, appears in the 1040 h sample and grows in intensity for the 1680 h sample. This peak is a dominant peak in the spectrum of the sodium uranyl oxide hydrate mineral clarkeite ($Na[(UO_2)O(OH)][H_2O]_{0-1}$). Clarkeite is isostructural with the synthetic anhydrous sodium uranates $Na_2U_2O_7$ and $Na_6U_7O_{24}$, and these phases are difficult to distinguish from one another with powder XRD (Finch and Ewing, 1997). Clarkeite or one of the sodium uranates was the only phase with an XRD peak at 15° that could have formed from the contents of the reaction flasks. The uranyl oxide hydrate schoepite ($[UO_2]_8O_2[OH]_{12} \cdot 12H_2O$) is a common secondary phase that might have been expected to form; however, the XRD patterns of the collected solids lack the characteristic schoepite peak at 12°.

The precipitation of a new solid phase following initial soddyite dissolution was also observed by SEM. In the electron micrographs taken after 1 h (Fig. 6a) and 365 h (Fig. 6b), blocky crystals of soddyite, ~1 by 2 μm, are the only solids observed. After 1683 h, a new phase in addition to soddyite is observed by SEM (Fig. 6c). The new phase consists of 1- to 2-μm-long needle-like crystals and appears as discrete particles not associated with the blocky soddyite crystals.

The Raman spectra of solids from the stock soddyite suspension and the conclusion of the batch dissolution experiment for synthesis 1 are presented in Figure 7a. The spectrum of the stock soddyite is consistent with a published spectrum in which the dominant peak at 829 cm^{-1} was assigned to the symmetric uranyl ion stretch; the peak at 457 cm^{-1} to the equatorial U-O stretch; and peaks at 222, 288, and 308 cm^{-1} to U-O bending modes (Biwer et al., 1990). The spectrum of the solids from the batch dissolution reactor contains the same peaks as the spectrum of the stock soddyite, but the dominant peak at 829 cm^{-1} is broader, and additional peaks are observed at 136 and 866 cm^{-1}. A weighted value of the stock soddyite spectrum was subtracted from the spectrum of the solids from the batch

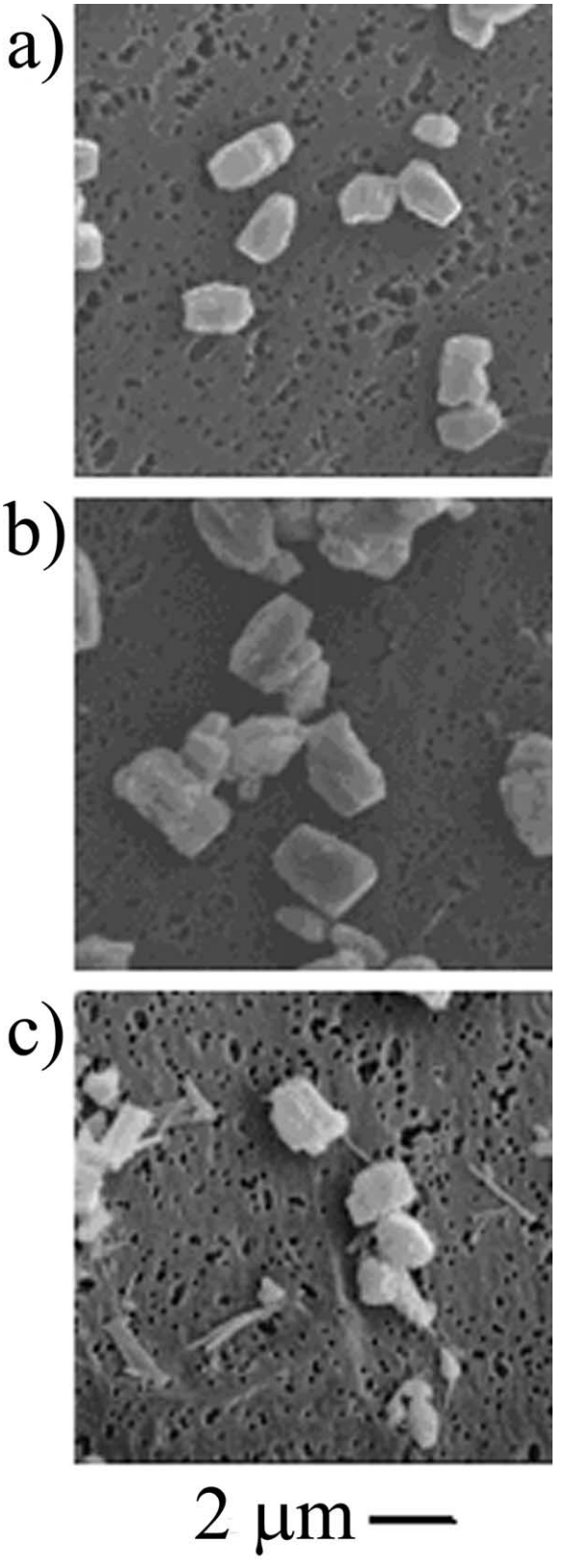

Fig. 6. Scanning electron micrographs of solids collected from batch dissolution experiments after (a) 1, (b) 365, and (c) 1683 h of reaction in batch reactors. Only the blocky soddyite crystals are observed after 1 and 365 h, but a new needle-shaped phase is apparent after 1683 h.

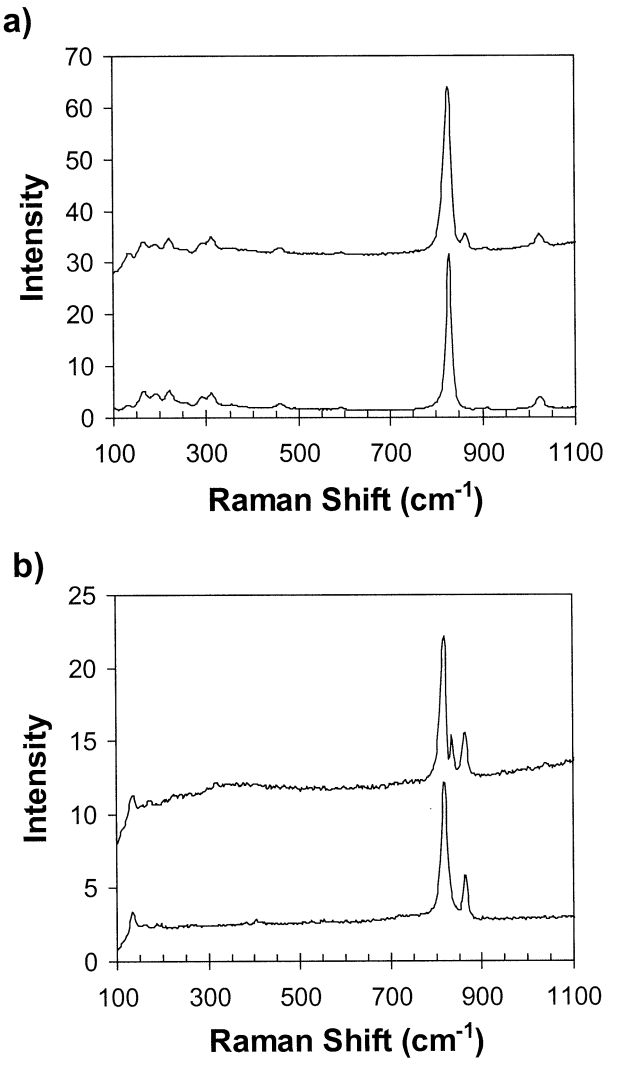

Fig. 7. Raman spectra of (a) solids at conclusion of batch dissolution (top) and synthetic soddyite stock (bottom). (b) Difference spectrum of batch solids - soddyite stock (top) and a synthetic sodium uranyl oxide hydrate (bottom). The dominant peak(s) in all spectra correspond to the symmetric stretch of the uranyl ion. In soddyite, the vibration occurs at 829 cm^{-1}, and in the synthetic uranyl oxide hydrate, the symmetric stretch shifts to 820 cm^{-1} and the asymmetric stretch appears at 866 cm^{-1}. Peaks below 500 cm^{-1} correspond to equatorial U-O stretches and U-O bending modes.

dissolution reactor; the difference spectrum, which exhibits peaks at 136, 820, and 866 cm^{-1}, is displayed in Figure 7b. The 866- and 820-cm^{-1} peaks are assigned to the antisymmetric and symmetric uranyl stretches, respectively. These peaks match perfectly with those from a separately synthesized solid phase that was identified as a clarkeite-like phase by XRD (Giammar, 2001). Unfortunately, no well-resolved published spectra are available for comparison; however, our measured antisymmetric stretch is consistent with the 870-cm^{-1} value determined for $Na_2U_2O_6(OH)_2$(s), which has the same Na/U ratio as clarkeite (Cejka, 1999).

3.3. Flow-Through Dissolution Experiments

Rates of soddyite dissolution were determined using flow-through reactors to avoid the accumulation of reaction products and the reprecipitation of U. The effluent U concentrations from the flow-through reactors over the course of the experiment were in the range from 0.91 to 1.27 μM for the reactor without added Si and in the range from 0.59 to 0.87 μM for the reactor with 100 μM dissolved Si in the influent (Fig. 8). The effluent pH from the reactors was consistently 6.00 to 6.06. Constant effluent composition indicates that steady-state dissolution has been reached. For the reactor without added Si, the effluent U concentrations were very stable for the first 80 reactor volumes but were higher in the last 4 samples. For the reactor with 100 μM dissolved Si in the influent, the effluent U concentrations remained stable for ~50 reactor volumes and then gradually decreased. As dissolved products were flushed from the reactors, the total U concentration remaining in the reactors decreased by 11.7 and 7.4% for the zero Si and 100 μM Si reactors, respectively. This would be expected to result in a small decrease in the release rates (and corresponding effluent U concentrations). Although the hydraulic residence times for the reactors were not entirely constant during the course of the experiments, the measured residence times were incorporated in calculating dissolution rates (using Eqn. 1). These variations do not account for the variability in observed effluent concentrations. Although this variability introduces some uncertainty into the calculated dissolution rates, average values of the steady-state rates of U release were determined to be 0.70 ± 0.11 μmol m^{-2} h^{-1} for the reactor without added Si and 0.45 ± 0.06 μmol m^{-2} h^{-1} for the reactor with 100 μM Si in the influent.

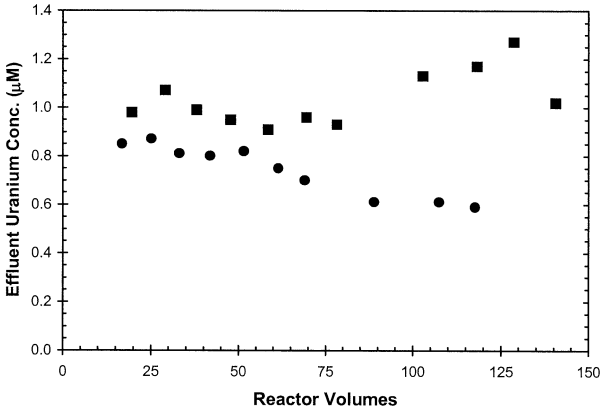

Fig. 8. Effluent U concentrations from flow-through reactors at pH 6 (5 mM 2-[n-morpholino]ethanesulfonic acid), 0.41 to 0.42 g L^{-1} soddyite ($[U]_T$ = 1.25 mM), ~1.3 h residence time, and with either 0 (■) or 100 μM (●) dissolved Si in the reactor influent.

4. DISCUSSION

4.1. Evolution of Dissolved Concentrations and Solid Phases

The dominant feature of the evolution of the dissolved U concentration in the batch experiments is the abrupt decrease to a constant value, which followed a period of increasing concentration. The changes in the dissolved U concentration can be interpreted qualitatively by considering the dissolution and precipitation of the original solid soddyite with rates $R_{diss}^{soddyite}$

and $R_{pptn}^{soddyite}$ and of the secondary sodium uranyl oxide hydrate phase (referred to herein as "clarkeite") with rates $R_{diss}^{clarkeite}$ and $R_{pptn}^{clarkeite}$, represented as follows:

$$\frac{d[U]_{diss}}{dt} = R_{diss}^{soddyite} - R_{pptn}^{soddyite} + R_{diss}^{clarkeite} - R_{pptn}^{clarkeite} \quad (2)$$

At the initiation of batch experiments, the dissolved U concentration increases as soddyite dissolves at the rate $R_{diss}^{soddyite}$. When the dissolved U concentration reaches the critical level necessary for "clarkeite" nucleation, precipitation of "clarkeite" proceeds at the rate $R_{pptn}^{clarkeite}$, which increases as the "clarkeite" crystals grow because of the increasing surface area for U uptake. Once $R_{pptn}^{clarkeite}$ exceeds $R_{diss}^{soddyite}$, the dissolved U concentration starts to decrease. However, the continuing release of Si (Fig. 3) indicates that soddyite has not reached equilibrium (i.e., $R_{diss}^{soddyite} > R_{pptn}^{soddyite}$). During the ongoing soddyite dissolution, the U released to solution from soddyite is rapidly taken up by the growing "clarkeite" phase (i.e., $R_{pptn}^{clarkeite} \gg R_{diss}^{soddyite}$). While net U transfer from soddyite to "clarkeite" occurs via release to solution and subsequent uptake from the dissolved phase, the dissolved U concentration was relatively stable in the range from 1.9 to 2.7 μM. This stable U concentration suggests that the "clarkeite" phase had reached pseudo-equilibrium (i.e., $R_{pptn}^{clarkeite} \approx R_{diss}^{clarkeite}$) and was controlling the dissolved U concentration. Eventually, the dissolved concentration of Si should also reach its equilibrium value, and the (net) dissolution of soddyite should cease. The expected behavior at equilibrium is discussed in sections 4.2 and 4.3.

Similar transient behavior, in which the dissolved U concentration exceeds or overshoots its final (equilibrium) concentration, was observed by Casas et al. (1994) upon addition of a natural uranophane sample to distilled water. The dissolved U concentration increased for the first 1800 h and then decreased dramatically at 2000 h to a value that remained constant for the duration of their experiment. In this case, U released during uranophane dissolution was taken up by precipitation of soddyite, the more stable phase at the low total calcium concentration of the suspension. In a prior study of soddyite dissolution at pH 6 in 0.1 M $NaClO_4$, measured dissolved U concentrations were observed to decline from ~10 μM at 60 d to 4 μM at 120 d, but formation of secondary phases could not be confirmed by XRD (Moll et al., 1996). Such transients have rarely been reported in other studies of mineral dissolution but were recently reported in a study of sanidine ($KAlSi_3O_8$) dissolution in 0.1 M $NaHCO_3$ solution (Alekseyev et al., 1997). The dissolved aluminum concentration reached a maximum during the congruent phase of sanidine dissolution and then decreased during an incongruent phase in which analcime ($NaAlSi_2O_6 \cdot H_2O$) precipitated.

Formation of "clarkeite" as a secondary solubility-controlling phase was the most significant finding from the batch dissolution studies. Although this phase was barely detectable by XRD after even 1040 h, it was already influencing the dissolved U concentration at 198 to 365 h. The XRD patterns and Raman spectra suggest that even at the conclusion of the batch dissolution experiment, the solubility-controlling phase was present as only a minor component. The predicted equilibrium distribution of solid-phase U between soddyite and "clarkeite" is discussed in section 4.3. The structure of clarkeite is based on sheets of edge-sharing uranyl bipyramidal polyhedra with Na^+ ions occupying the interlayer positions (Finch and Ewing, 1997). This structure is distinct from the framework structure of soddyite; therefore, it is likely that "clarkeite" precipitation occurs by the uptake of U from solution by discrete "clarkeite" crystals, not by reordering of the soddyite structure. Nucleation may be facilitated by soddyite surfaces or vessel walls, but "clarkeite" crystals ultimately grow as a distinct phase, as demonstrated by SEM.

4.2. Equilibrium Soddyite Solubility

Before examining the possible coexistence of soddyite and "clarkeite" phases and the rates of dissolution, it is useful to examine the predicted dissolved concentrations of U and Si at equilibrium with soddyite. This equilibrium is calculated assuming stoichiometric dissolution of the solid (Eqn. 3) with an associated solubility product constant (Eqn. 4; Nguyen et al., 1992):

$$(UO_2)_2SiO_4 \cdot 2H_2O_{(s)} + 4H^+ = 2UO_2^{2+} + SiO_2(aq) + 4H_2O \quad (3)$$

$$K_{sp} = \frac{\{UO_2^{2+}\}^2 \{SiO_2(aq)\}}{\{H^+\}^4} \quad (4)$$

Several solubility constants have been reported for soddyite (Nguyen et al., 1992; Moll et al., 1996; Pérez et al., 1997). Interpretation and application of these constants is complicated by the difficulty in relating the activity of UO_2^{2+} to the measured dissolved U concentration. Above pH 4, the hydrolysis species of uranyl contribute significantly to the total dissolved U, and in systems open to atmospheric carbon dioxide, dissolved uranyl carbonate species become significant above pH 6 and begin dominating speciation between pH 7 and 8. Despite the publication of a compilation of thermodynamic data for U (Grenthe et al., 1992), the set of solution reactions considered varies from study to study. Previously published solubility constants and the conditions for which they were determined are compiled in Table 2, which also includes soddyite solubility constants recalculated from the published raw data using a comprehensive set of complexation reactions (Table 1) and the Davies (1962) equation for making ionic strength corrections.

A solubility product of log $K_{sp} = 5.74 \pm 0.21$ was determined for soddyite equilibrated at pH 3 under argon using the Nuclear Energy Agency database (Grenthe et al., 1990) to calculate uranyl speciation and the specific ion interaction theory (SIT) to correct for ionic strength (Nguyen et al., 1992). In another study conducted over a pH range of 3 to 9 and under both air and nitrogen atmospheres, Moll et al. (1996) were unable to model their complete data set using a single solubility product. However, at pH 3, solubility products of log $K_{sp} = 6.03 \pm 0.45$ (under N_2) and 6.15 ± 0.53 (in air) were calculated considering only the $\{UO_2^{2+}\}$ species and correcting for ionic strength with the SIT. As shown in Table 2, a recalculation of these values with a consistent set of complexation reactions and ionic strength corrections gives a range of solubility products (log K_{sp} between 5.35 and 5.50) that are well within the estimated errors. The recalculated value of Nguyen et al. (1992)

Table 2. Conditions and results of previous determinations of the soddyite solubility product.

Experimental conditions[a]							Log K_{sp}		
pH	atm	I (mM)	$[U]_{diss}$ (μM)	$[Si]_{diss}$ (μM)	Added solutes	U species considered[b]	Published	Recalculate[d]	Reference[c]
3.0	Ar	80	19.3	5.12		UO_2^{2+} $(UO_2)_2(OH)_2^{2+}$	5.74 ± 0.21	5.35	1
3.0	N_2	140	18.0 (N_2)	9.00 (N_2)	0.1 M $NaClO_4$	UO_2^{2+}	6.03 ± 0.45(N_2)	5.39 (N_2)	2
	Air		19.5 (air)	10.0 (air)			6.15 ± 0.53(air)	5.50 (air)	
8.54 to 9.11	Air	9 to 33	0.29 to 2.24	Calculated[f]	1 to 20 mM $NaHCO_3$ 1 mM Na_2SiO_3 7 mM$NaClO_4$	SKB database[g]	2.58 to 6.36	2.76 to 6.99	3

[a]All experiments listed were conducted as batch experiments.
[b]Only species considered in the cited references and present as more than 1% of dissolved U are listed.
[c]All of the authors adjusted conditional constants to $I = 0$ using the specific ion interaction theory discussed in Grenthe et al. (1992).
[d]Recalculated in this work using the entire database of constants in Table 1 and correcting for ionic strength with the Davies (1962) equation.
[e](1) Nguyen et al. (1992), (2) Moll et al (1996), (3) Pérez et al. (1997).
[f]Calculated as the sum of the initial dissolved Si (1 mM) and that released assuming congruent dissolution of the soddyite (i.e., $0.5[U]_{diss}$).
[g]Puigdomenech and Bruno (1988).

(log $K_{sp} = 5.35$) will be used in the discussion that follows for interpretation of the current experimental data.

Pérez et al. (1997) investigated the solubility of soddyite at higher pH and in the presence of dissolved carbonate, using the SKBU database (Puigdomenech and Bruno, 1988) to calculate dissolved uranyl speciation. Their solubility product determination was highly sensitive to the HCO_3^- concentration, and they reported a range for log K_{sp} from 2.58 to 6.36, with an average of 3.9 ± 0.7 for HCO_3^- concentrations >2 mM (Pérez et al., 1997). Using the raw data of Pérez et al. (1997), the constants of Table 1, and the Davies (1962) equation, we were also unable to calculate a single log K_{sp} that fit their entire data set. These failures to calculate a single solubility product for this data set suggest that either the systems measured were not at equilibrium or the sets of complexation reactions used by us in our recalculation or originally by Pérez et al. (1997) to calculate the uranyl ion activity overestimate the extent of uranyl complexation at high carbonate concentrations.

To put our results in the context of the published solubility products, the reaction quotient was calculated for the conditions in the batch experiment immediately before the reprecipitation event. For the soddyite from synthesis 1, these conditions (at $t = 365$ h) are pH 6, 0.012 M ionic strength, $P_{CO_2} = 10^{-3.5}$ atm, 4.3 μM dissolved Si, and 9.1 μM dissolved U ($UO_2^{2+} = 1.84 \times 10^{-7}$ M). A reaction quotient of log $Q = 5.16$ was calculated, indicating that the suspension was still undersaturated with respect to soddyite at the time of "clarkeite" precipitation. The use of $P_{CO_2} = 10^{-3.5}$ atm is an upper limit that assumes equilibrium with atmospheric CO_2, whereas a CO_2-free system offers a lower limit. For the experimental conditions of this study, speciation calculations are highly insensitive to the value of P_{CO_2} in this range; for $P_{CO_2} = 0$, UO_2^{2+} would equal 1.85×10^{-7} M, and log Q would equal 5.17. For congruent dissolution and a solubility product of log $K_{sp} = 5.35$, the dissolved U concentration in equilibrium with soddyite is 11.3 μM (in the absence of any secondary phases). In the other published study of soddyite solubility at pH 6 in an open system (in 0.1 M $NaClO_4$), the dissolved U concentration was ~10 μM at equilibrium (Moll et al., 1996).

4.3. Predicted Equilibrium of Mixed Solid System

At the conclusion of the batch experiments, XRD and Raman spectroscopy identify both soddyite and a clarkeite-like phase. The coexistence of both phases at equilibrium in a system open to atmospheric carbon dioxide does not violate Gibbs phase rule. It is instructive to calculate the solution composition in equilibrium with both soddyite (using the solubility product from Eqn. 4) and "clarkeite." The dissolution of "clarkeite" (written as $Na[UO_2]O[OH](s)$, omitting waters of hydration for convenience) is represented by Eqn. 5, with the solubility product shown in Eqn. 6:

$$3H^+ + Na(UO_2)O(OH)_{(s)} = Na^+ + \{UO_2^{2+}\} + 2H_2O \quad (5)$$

$$K_{sp} = \frac{\{UO_2^{2+}\}\{Na^+\}}{\{H^+\}^3} \quad (6)$$

Solubility products have been reported for synthetic anhydrous Na uranates, but not for clarkeite. To examine the possible coexistence of soddyite and "clarkeite," the predicted equilibrium of the batch reactors is shown in Fig. 9 as a function of the "clarkeite" solubility product using the recalculated soddyite solubility product of Nguyen et al. (1992) (log $K_{sp} = 5.35$). Soddyite and "clarkeite" can coexist for log $K_{sp,\ clarkeite}$ between 8.55 and 9.35. The measured equilibrium dissolved U concentration of 2.2 μM corresponds to a log $K_{sp,\ clarkeite}$ of 9.02. For this "clarkeite" solubility, the equilibrium dissolved Si concentration is 24.4 μM, and the solid phase U is distributed between "clarkeite" (47 μM) and soddyite (311 μM). A distribution of solid-phase U strongly biased toward soddyite is consistent with XRD and Raman measurements, in which the peaks representing "clarkeite" are considerably smaller than those representing soddyite.

It is interesting to note that while the solid-phase U is predominantly in the soddyite phase, the dissolved U concentration is significantly lower than it would be were it in equilibrium with soddyite alone. The dissolved U concentration is

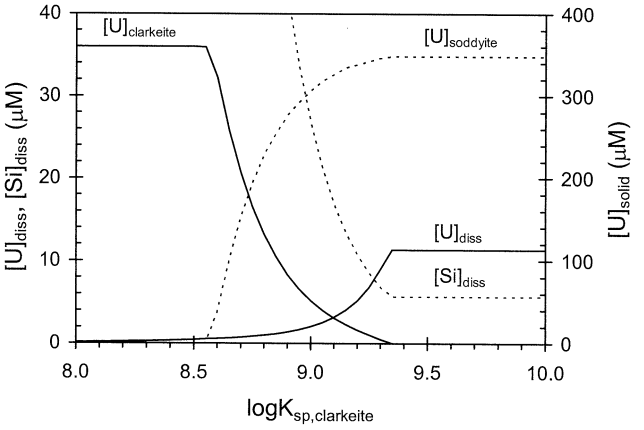

Fig. 9. Dissolved U and Si concentrations and U concentration in soddyite and "clarkeite" as a function of log $K_{sp,\ clarkeite}$ for $[U]_T = 360$ μM, $[Si]_T = 180$ μM, $I = 12.3$ mM, $P_{CO_2} = 10^{-3.5}$ atm, and log $K_{sp,\ soddyite} = 5.35$. "Clarkeite" and soddyite coexist for log $K_{sp,\ clarkeite} = 8.55$ to 9.35.

controlled by the minor "clarkeite" phase. The overall hierarchy of total element concentrations is Na > U > Si. Following this hierarchical approach, the high Na concentration and the "clarkeite" solubility product fix the dissolved U concentration. The dissolved Si is then fixed by the dissolved U concentration and the soddyite solubility product.

The preceding discussion indicates the potential importance of Na, often considered a background cation, in determining U solubility and mobility. In a recent series of laboratory experiments reacting U(VI) with an array of solids, a clarkeite-like solid was formed in experiments conducted at high dissolved Na, even in the presence of 0.01 M Na_2CO_3 (Yamakawa and Traina, 2001). Although clarkeite is formed in nature at high temperature during pegmatite crystallization (Finch and Ewing, 1997), formation of a clarkeite-like solid at low temperature may control the dissolved U concentration in systems with high Na concentrations.

4.4. Quantification of Soddyite Dissolution Rates

The dissolution rate calculated from the flow-through experiment without added Si is 0.71 μmol U m^{-2} h^{-1} (or $10^{-10.0}$ mol Si m^{-2} s^{-1}), which is within the range ($10^{-8.0}$ to $10^{-13.4}$ mol m^{-2} s^{-1}) reported for silicate and aluminosilicate minerals at pH 5 and is comparable to the weathering rate of forsterite, Mg_2SiO_4 (Langmuir, 1997). In this flow-through experiment, soddyite dissolution occurs under conditions that are very undersaturated with respect to the solid. On the basis of the measured pH of 6.0 and average dissolved U concentration of 1.0 μM and assuming a stoichiometric dissolved Si concentration of 0.5 μM, the saturation index (log Q/K_{sp}) is -2.10.

A slower dissolution rate of 0.44 μmol U m^{-2} h^{-1} was observed in the flow-through reactor with 100 μM added Si. The 100 μM dissolved Si concentration is somewhat lower than the median value ($\sim$270 μM) for groundwater (Langmuir, 1997). The conditions in this reactor are much closer to equilibrium, with an average dissolved U concentration of 0.74 μM, corresponding to a saturation index of -0.01 relative to log K_{sp} = 5.35. Dissolved U concentrations range from 0.87 μM early in the experiment to a nearly constant value of 0.60 μM after 70 reactor volumes. The range of dissolved U corresponds to a saturation index from -0.11 to 0.14, again relative to a log K_{sp} of 5.35. As discussed in section 4.2, reasonable values for log K_{sp} are 5.35 to 5.50. The dependence of net dissolution rate (R_{net}) on the Gibbs free energy of a reaction has been recently reviewed by Lasaga (1998) and is expressed by Eqn. 7, where k and n are constants:

$$R_{net} = k\left(1 - \exp\left(\frac{n\Delta G}{RT}\right)\right) \quad (7)$$

For $n = 1$ (applicable to elementary reactions), the net reaction rate decreases sharply as the reaction approaches equilibrium.

The rate of U release from soddyite in the batch experiments, however, was an order of magnitude slower than the rate observed in the flow-through experiments. The saturation index for soddyite in the batch experiments ranged from -0.43 (synthesis 2) to -0.19 (synthesis 1) immediately before precipitation of the secondary phase and reached -0.43 after the secondary phase had formed (i.e., at pH 6 with 2 μM dissolved U and 10 μM dissolved Si). The linear increase with time in both the concentrations of dissolved U (before secondary phase formation) and Si (both before and after secondary phase formation) correspond to release rates of 0.064 μmol U m^{-2} h^{-1} and 0.035 μmol Si m^{-2} h^{-1}. Since the conditions in the batch experiments are actually slightly more energetically favorable for (net) soddyite dissolution than those in the 100 μM Si flow-through reactor, the slower dissolution rate observed in the batch reactor cannot be attributed to a decreasing net dissolution rate as reaction products accumulate. This discrepancy suggests that dissolution in the batch reactor may be transport limited.

Rates of soddyite dissolution in HCO_3^- solutions determined from batch experiments have been reported by Pérez et al. (1997). However, the interpretation of the kinetic data in this study relied on equilibrium constants of questionable validity (as discussed in section 4.2). Therefore, direct comparison with our results would not be appropriate.

5. CONCLUSIONS

Batch and flow-through soddyite experiments have examined the dissolution behavior of soddyite, an important mineral phase in the paragenesis of U ore deposits and spent nuclear fuel. The most striking feature of the batch experiments was the precipitation of a clarkeite-like secondary phase. While nucleation of the clarkeite-like phase may have occurred at the soddyite surface or on the walls of the reaction flask, the secondary phase ultimately grew as discrete crystals, not by a transformation of existing soddyite crystals. The onset of precipitation of this secondary phase occurred as soddyite dissolution progressed and was accompanied by a significant decrease in the dissolved U concentration. Thus, the dissolved U concentrations in the batch experiments exhibited a transient maximum value in approximately fivefold excess of the steady-state value controlled by the solubility of the clarkeite-like phase. During the transfer of U from one phase to the next in a paragenetic sequence, such transients in the dissolved U concentrations may allow greater mobilization of U than would

be expected on the basis of equilibrium solubilities. Overall U release may be significantly underpredicted if the rates of dissolution and precipitation reactions are not considered.

A reinterpretation of existing equilibrium soddyite solubility data with a single set of dissolved complexation reactions supports the solubility product determined previously by Nguyen et al. (1992), which is also consistent with the results of this work. While soddyite solubility had been previously studied, the kinetics of soddyite dissolution had received less attention. Here, we report a steady-state dissolution rate for soddyite, obtained in a flow-through reactor at pH 6, of 0.71 μmol U m^{-2} h^{-1}, comparable to that of the silicate mineral forsterite, Mg_2SiO_4. Introduction of 100 μM Si into the influent of the flow-through reactor decreased the observed (net) dissolution rate by a factor of 1.6. In this experiment, the conditions were much closer to soddyite saturation, which is reflected in the decreased (net) dissolution rate. These results suggest that soddyite dissolution could be significantly inhibited in groundwater because of ambient dissolved Si concentrations. Possible effects on dissolution kinetics of parameters not examined in this study (specifically, carbonate concentration, pH, and ionic strength) deserve further investigation.

Perhaps more significantly, the importance of the dissolved Na concentration on secondary mineral formation has been identified. In environments with high Na concentrations, a clarkeite-like sodium uranyl oxide hydrate phase may form following the dissolution of other uranyl phases and should be considered as a potential solubility-limiting phase. While sufficient Na concentrations for clarkeite formation may not be common in natural environments, clarkeite-like phases may be expected in soils and sediments contaminated by U-laden aqueous wastes with high dissolved Na concentrations. Such conditions are encountered under some waste storage tanks at the Hanford Nuclear Reservation in Washington State.

Acknowledgments—The Raman measurements were suggested by George Rossman and performed on an instrument in his laboratory. The assistance of Liz Arredondo in the acquisition of Raman spectra is greatly appreciated. We appreciate the efforts of the associate editor and three anonymous reviewers, whose constructive comments helped to improve the quality of this paper.

Associate editor: G. Sposito

REFERENCES

Alekseyev V. A., Medvedeva L. S., Prisyagina N. I., Meshalkin S. S., and Balabin A. I. (1997) Change in the dissolution rates of alkali feldspars as a result of secondary mineral precipitation and approach to equilibrium. *Geochim. Cosmochim. Acta* **61,** 1125–1142.

Biwer B. M., Ebert W. L., and Bates J. K. (1990) The Raman spectra of several uranyl-containing minerals using a microprobe. *J. Nucl. Mater.* **175,** 188–193.

Burns P. C. (1999) The crystal chemistry of uranium. In *Uranium: Mineralogy, Geochemistry and the Environment* (eds. P. C. Burns and R. Finch), *Rev. Mineral.* **38,** 23–90. Mineralogical Society of America, Washington, DC.

Casas I., Bruno J., Cera E., Finch R. J., Ewing R. C. (1994) *Kinetic and Thermodynamic Studies of Uranium Minerals: Assessment of the Long-Term Evolution of Spent Nuclear Fuel*. SKB Technical Report 94–16.

Casas I., de Pablo J., Gimenez J., Torrero M. E., Bruno J., Cera E., Finch R. J., and Ewing R. C. (1998) The role of pe, pH, and carbonate on the solubility of UO_2 and uraninite under nominally reducing conditions. *Geochim. Cosmochim. Acta* **62,** 2223–2231.

Cejka J. (1999) Infrared spectroscopy and thermal analysis of the uranyl minerals. In *Uranium: Mineralogy, Geochemistry and the Environment* (eds. P. C. Burns and R. Finch), *Rev. Mineral.* **38,** 521–560. Mineralogical Society of America, Washington, DC.

Davies C. W. (1962) *Ion Association*. Butterworths, Washington, DC.

de Pablo J., Casas I., Gimenez J., Molera M., Rovira M., Duro L., and Bruno J. (1999) The oxidative dissolution mechanism of uranium dioxide. I. The effect of temperature in hydrogen carbonate medium. *Geochim. Cosmochim. Acta* **63,** 3097–3103.

Environmental Research Software. (1998) MINEQL$^+$: A Chemical Equilibrium Modeling System, Version 4.0. Environmental Research Software, Hallowell, ME.

Finch R., Murakami T. (1999) Systematics and paragenesis of uranium minerals. In *Uranium: Mineralogy, Geochemistry and the Environment* (eds. P. C. Burns and R. Finch), *Rev. Mineral.* **38,** 91–180. Mineralogical Society of America, Washington, DC.

Finch R. J. and Ewing R. C. (1997) Clarkeite: New chemical and structural data. *Am. Mineral.* **82,** 607–619.

Finn P. A., Hoh J. C., Wolf S. F., Slater S. A., and Bates J. K. (1996) The release of uranium, plutonium, cesium, strontium, technetium and iodine from spent fuel under unsaturated conditions. *Radiochim. Acta* **74,** 65–71.

Giammar D. E. (2001) Geochemistry of Uranium at Mineral-Water Interfaces: Rates of Sorption-Desorption and Dissolution-Precipitation Reactions. Ph.D. thesis. California Institute of Technology, Pasadena.

Good N. E., Winget G. D., Winter W., Connolly T. N., Izawa S., and Singh R. M. M. (1966) Hydrogen ion buffers for biological research. *Biochemistry* **5,** 467–477.

Grenthe I., Fuger J., Konings R. J. M., Lemire R. J., Mueller A. B., Nguyen-Trung C., and Wanner H. (1990) *Chemical Thermodynamics of Uranium*. Nuclear Energy Agency, Organisation for Economic Co-operation and Development, Gif-sur-Yvette, France.

Grenthe I., Fuger J., Konings R. J. M., Lemire R. J., Mueller A. B., Nguyen-Trung C., and Wanner H. (1992) *Chemical Thermodynamics of Uranium*. Nuclear Energy Agency, Organisation for Economic Co-operation and Development, Elsevier, Amsterdam, the Netherlands.

Ildefonse P., Muller J. -P., Clozel B., and Calas G. (1990) Study of two alteration systems as natural analogues for radionuclide release and migration. *Eng. Geol.* **29,** 413–429.

Joint Committee on Powder Diffraction Standards–International Centre for Diffraction Data. (1999) Powder diffraction file. International Centre for Diffraction Data, Newtown Square, PA.

Langmuir D. (1997) *Aqueous Environmental Geochemistry*. Prentice Hall, Upper Saddle River, NJ.

Lasaga A. C. (1998) *Kinetic Theory in the Earth Sciences*. Princeton University Press, Princeton, NJ.

Moll H., Matz W., Schuster G., Brendler E., Bernhard G., and Nitsche H. (1995) Synthesis and characterization of uranyl orthosilicate $(UO_2)_2SiO_4$-H_2O. *J. Nucl. Mater.* **227,** 40–49.

Moll H., Geipel G., Matz W., Bernhard G., and Nitsche H. (1996) Solubility and speciation of $(UO_2)_2SiO_4$-H_2O. *Radiochim. Acta* **74,** 3–7.

Nguyen S. N., Silva R. J., Weed H. C., and Andrews Jr. J. E. (1992) Standard Gibbs free energies of formation at the temperature 303.15K of four uranyl silicates: Soddyite, uranophane, sodium boltwoodite, and sodium weeksite. *J. Chem. Thermodynam.* **24,** 359–376.

Pearcy E. C., Prikryl J. D., Murphy W. M., and Leslie B. W. (1994) Alteration of uraninite from the Nopal I deposit, Peña Blanca District, Chihuahua, Mexico, compared to degradation of spent nuclear fuel in the proposed U.S. high-level nuclear waste repository at Yucca Mountain, Nevada. *Appl. Geochem.* **9,** 713–732.

Pérez I., Casas I., Torrero M. E., Cera E., Duro L., and Bruno J. (1997) Dissolution studies of soddyite as a long-term analogue of the oxidative alteration of the spent nuclear fuel matrix. *Materials Research Society Symposia Proceedings Vol. 465, Scientific Basis for Nuclear Waste Management XX*. In: (eds. W. J. Gray and I. R. Triay). Materials Research Society, Pittsburgh, PA, pp. 565–572.

Puigdomenech I., Bruno J. (1988) Modelling Uranium Solubilities in Aqueous Solutions: Validation of the Thermodynamic Database for EQ3/6 Geochemical Codes. SKB Technical Report 88–21.

Satoh I. and Choppin G. R. (1992) Interaction of uranyl(VI) with silicic acid. *Radiochim. Acta* **56,** 85–87.

Shoesmith D. W. (2000) Fuel corrosion processes under waste disposal conditions. *J. Nucl. Mater.* **282,** 1–31.

Silva R. J. (1992) Mechanisms for the retardation of uranium (VI) migration. *Mat. Res. Soc. Symp. Proc.* **257,** 323–330.

Soares H. M. V. M., Conde P. C. F. L., Almeida A. A. N., and Vasconcelos M. T. S. D. (1999) Evaluation of n-substituted aminosulfonic acid pH buffers with a morpholino ring for cadmium and lead specation studies by electroanalytical techniques. *Anal. Chim. Acta* **394,** 325–335.

Steward S. A. and Mones E. T. (1997) Comparison and modeling of aqueous dissolution rates of various uranium oxides. In *Materials Research Society Symposia Proceedings Vol. 465, Scientific Basis for Nuclear Waste Management XX*. (eds. W. J. Gray and I. R. Triay). Materials Research Society, Pittsburgh PA, pp. 557–564.

Torrero M. E., de Pablo J., Sandino M. C. A., and Grambow B. (1994) A comparison between unirradiated $UO_{2(s)}$ and schoepite solubilities in 1M NaCl medium. *Radiochim. Acta* **66/67,** 29–35.

Trocellier P., Cachoir C., and Guilbert S. (1998) Dissolution of uranium dioxide in granitic groundwater by secondary phase formation. *J. Nucl. Mater.* **256,** 197–206.

Vochten R., Van Haverbeke L., Van Springel K., and De Grave E. (1995) Soddyite: Synthesis under elevated temperature and pressure, and study of some physicochemical characteristics. *N. Jb. Miner. Mh.* **10,** 470–480.

Wronkiewicz D., Buck E. (1999) Uranium mineralogy and the geologic disposal of spent nuclear fuel. In *Uranium: Mineralogy, Geochemistry and the Environment* (eds. P. C. Burns and R. Finch), *Rev. Mineral.* **38,** 475–498. Mineralogical Society of America, Washington, DC.

Wronkiewicz D. J., Bates J. K., Gerding T. J., Veleckis E., and Tani B. S. (1992) Uranium release and secondary phase formation during unsaturated testing of UO_2 at 90°C. *J. Nucl. Mater.* **190,** 107–127.

Wronkiewicz D. J., Bates J. K., Wolf S. F., and Buck E. C. (1996) Ten-year results from unsaturated drip tests with UO_2 at 90°C: Implications for the corrosion of spent nuclear fuel. *J. Nucl. Mater.* **238,** 78–95.

Yamakawa I., Traina S. J. (2001) Precipitation processes of uranium in highly alkaline solutions: Possible chemical reactions occurring in the Hanford vadose zone. *Abstr. Papers Am. Chem. Soc.* **222,** part 1, GEOC-55.